OCEAN CHEMISTRY

Biological uptake and reversible scavenging of zinc in the global ocean

Thomas Weber[1]*†, Seth John[2]†, Alessandro Tagliabue[3], Tim DeVries[4]

Zinc (Zn) is a key micronutrient for marine phytoplankton, with a global distribution that is similar to silicic acid. The processes that govern this relationship, despite the very different biological cycling of Zn and silica, remain poorly understood. Here, we use diagnostic and mechanistic models to show that only a combination of Southern Ocean biological uptake and reversible scavenging of Zn onto sinking particles can explain the observations. The distinction between organic and adsorbed Zn can also reconcile the vertical distribution and mass balance of Zn isotopes, which previously appeared at odds. This holistic understanding explains the Zn deficiencies observed throughout the low-latitude ocean and implies a greater sensitivity of the marine Zn cycle to climate-driven changes in organic matter cycling than previously recognized.

Zn is the second most abundant micronutrient in phytoplankton biomass (*1*), with fundamental roles in DNA replication and transcription and as a cofactor in carbonic anhydrase and alkaline phosphatase enzymes (*2*). Since the earliest trace metal clean observations (*3*), and further exemplified by the global GEOTRACES program (*4*), a close correlation between the oceanic distributions of Zn and silicic acid [$Si(OH)_4$ (Si) hereafter] has been observed (Fig. 1A). Like Si, Zn is systematically enriched in deep water masses and deficient in intermediate water masses relative to other algal nutrients, such as phosphate (PO_4^{3-}). This results in widespread Zn scarcity throughout the low-latitude ocean, potentially affecting biological activity and plankton community structure, particularly in low PO_4^{3-} regions (*5*, *6*).

The spatial covariation of Zn and Si is surprising given their distinct biogeochemical cycles. Si is assimilated by diatoms and used to build external opal frustules, whereas Zn is assimilated by all phytoplankton taxa, with cellular quotas that scale with Zn availability up to ~10 mmol Zn per mol P (*7*). Only 1 to 3% of cellular Zn is directly incorporated into the frustules of cultured diatoms (*8*), whereas the vast majority is colocated with phosphorus (P) in internal organelles (*1*). Zn is released from decomposing organic particles at the same rate as P (*9*), and both are released shallower in the water column than Si (*10*, *11*). These observations suggest a fundamental decoupling between Zn and Si during the vertical cycling of organic matter that appears at odds with their correlated ocean concentrations (Fig. 1A). Identifying the "missing" processes that facilitate this linkage is essential to understand the climate sensitivity of the marine Zn cycle.

Recently, it has been hypothesized that the global Zn/Si covariation emerges from physical coupling in the Southern Ocean (*12*). As upwelling deep water flows northward in the region, surface Zn and Si are exhausted earlier than PO_4^{3-} (*13*). This results in a band of Zn- and Si-deficient water in the Polar Frontal Zone that is subducted northward within Antarctic Intermediate Water (AAIW), while Zn and Si remain enriched in Antarctic Bottom Water (AABW) that flows north from Antarctica at greater depth (*14*). Because these water masses ventilate much of the ocean interior, the stoichiometry of their formation regions is thought to propagate globally and overwhelm differences in organic Zn and Si cycling.

If the "Southern Ocean hypothesis" is complete, Zn concentrations must be modified very little as water masses spread northward beyond the Southern Ocean. Any significant accumulation of remineralized Zn would drive a shallower concentration maximum, making the Zn distribution diverge from Si and converge toward PO_4^{3-}.

We tested this hypothesis from an observational perspective by taking a representative observed profile of [Zn] from the North Pacific Ocean (Fig. 1B) and dividing it analytically into two components. The first component represents the quantity of Zn transported from the Southern Ocean to the North Pacific site (Fig. 1C) and was computed using a data-constrained ocean circulation model to propagate the Zn distribution of the Southern Ocean (statistically mapped south of 40°S) throughout the Pacific Ocean interior (*15*). The difference between the circulated component and the observed [Zn] then

[1]Department of Earth and Environmental Sciences, University of Rochester, Rochester, NY 14618, USA. [2]Department of Earth Sciences, University of Southern California, Los Angeles, CA 90089, USA. [3]School of Environmental Sciences, University of Liverpool, Liverpool, UK. [4]Department of Geography and Earth Research Institute, University of California, Santa Barbara, CA, USA.
*Corresponding author. Email: t.weber@rochester.edu
†These authors contributed equally to this work.

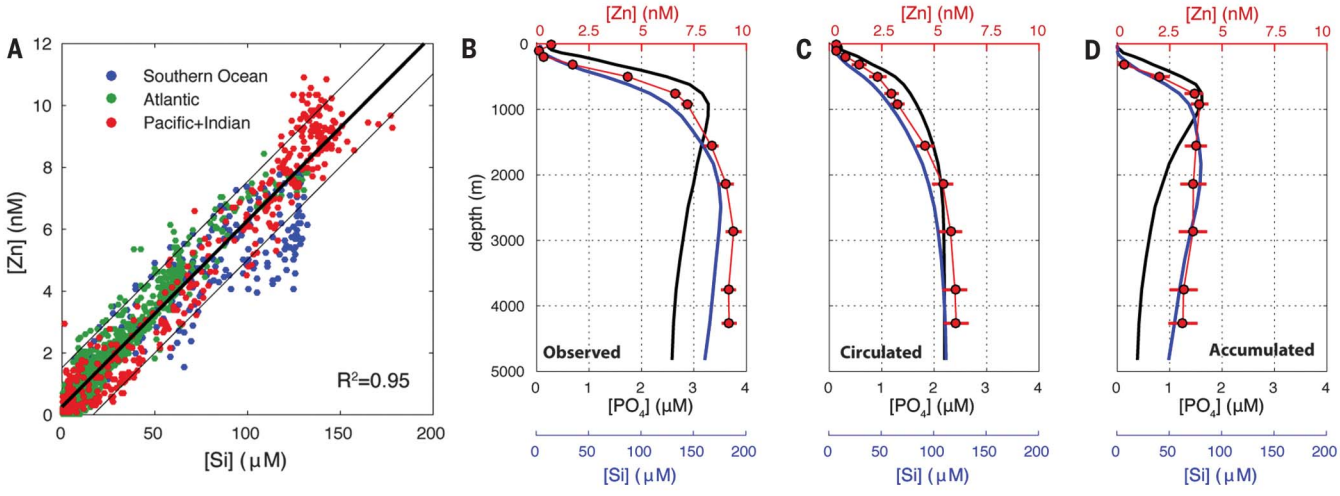

Fig. 1. Oceanic Zn distribution and components. (**A**) Scatter plot of observed Zn versus Si, with best-fit regression line (thick black line) and 95% prediction intervals (thin black lines). Zn data are from the GEOTRACES IDP 2014 and (*9*, *21*, *31*). (**B**) Observed profiles of Zn, Si, and PO_4^{3-} in the North Pacific Ocean (30°N, 140°W) (*9*). These profiles are divided into a component transported from the Southern Ocean (**C**) and a component accumulated by water masses since leaving the Southern Ocean (**D**). Uncertainty in each component was quantified using a Monte Carlo method (*15*).

quantifies the additional Zn that has accumulated during northward transport from the Southern Ocean—e.g., from remineralization or other internal cycling processes (Fig. 1D).

Our analysis reveals that only ~6 nM (~65%) of the observed Zn in the deep North Pacific is accounted for by circulation from the Southern Ocean (Fig. 1C). Therefore, ~3 nM (~35%) is unaccounted for and must have accumulated since these waters passed 40°S (Fig. 1D). Conducting a similar exercise for Si and PO_4^{3-} profiles (*15*) reveals that the accumulated Zn component does not share the same depth profile as accumulated PO_4^{3-}, which reaches a shallow peak centered around ~800 m, but rather exhibits a broad deep peak between 1000 and 3000 m, similar to accumulated Si (Fig. 1D). The same pattern is found repeating this analysis in the Tropical Pacific (fig. S1).

To further assess the role of the Southern Ocean, we developed a mechanistic model of global PO_4^{3-}, Zn, and Si cycling embedded within our data-constrained circulation model (*15*). Surface [PO_4^{3-}] and [Si] are restored toward observations to quantify the export of particulate organic P and biogenic Si, which remineralize over depth scales that were optimized to best match observed global PO_4^{3-} and Si distributions (fig. S2 and table S1). Zn complexation by organic ligands is represented by an equilibrium model (*16*), and biological uptake of uncomplexed Zn is coupled to PO_4^{3-} in a ratio that increases with [Zn] (*7*). Particulate organic Zn is assumed to remineralize over the same depth scale as organic P. Four parameters governing Zn complexation and uptake were optimized to best fit a range of observational constraints (*4*), including a Southern Ocean surface [Zn] transect and profiles from the Atlantic, Pacific, Indian, and Southern Oceans (fig. S3 and table S2). The optimization procedure is an important facet of our approach, allowing us to interpret remaining model-data discrepancies as genuine model deficiencies, rather than poor parameter choices.

Our optimized model produces a near-linear relationship between Zn and Si (Fig. 2A) when Southern Ocean surface [Zn] is accurately reproduced (Fig. 2B). However, the correlation (R^2 = 0.86) is weaker than observed (R^2 = 0.95) and systematic biases are evident, contrary to results of a previous modeling study (*12*). Modeled [Zn] is overestimated at low Si concentrations in intermediate water masses (Fig. 2, A and C) and underestimated in deep waters of the Pacific and Indian Oceans (Fig. 2C and fig. S3). Furthermore, our model requires Zn:P export ratios approaching 20 mmol:1 mol in order to sufficiently deplete [Zn] in the Southern Ocean (Fig. 2B and fig. S4), which exceeds the observed biological range (*1*).

Taken together, our diagnostic results and mechanistic modeling demonstrate that Southern Ocean uptake and circulation are important but insufficient factors to explain the global Zn distribution. Soft organic tissue cycling causes Zn to accumulate too shallowly in the water column, indicating that an additional process is required to explain the deep accumulation pattern

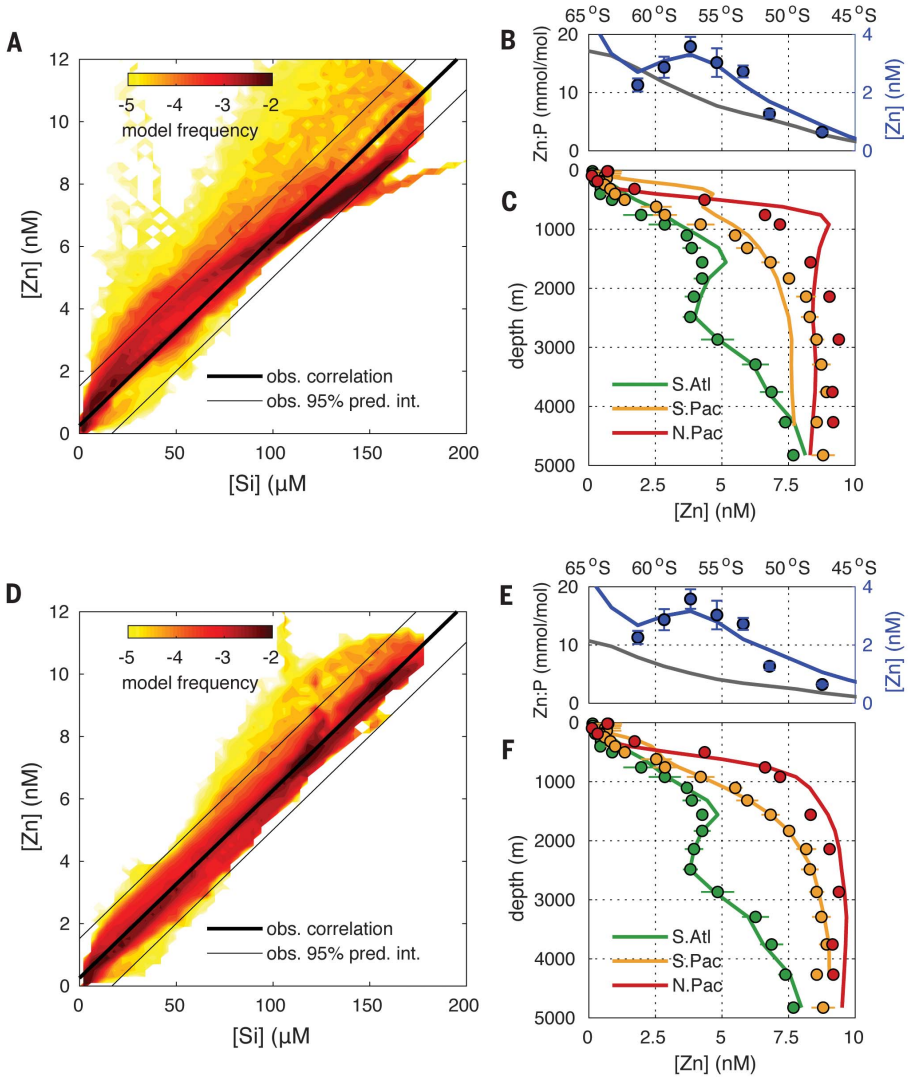

Fig. 2. Mechanistic models of Zn cycling. (**A** to **C**) Model representing the Southern Ocean Zn-Si hypothesis, with optimized surface Zn uptake. (**D** to **F**) Model that resolves reversible scavenging of Zn onto sinking particles. Models are evaluated against the observed Zn versus Si correlation [(A) and (D)], Southern Ocean surface distribution [(B) and (E)], and Atlantic and Pacific profiles [(C) and (F)]. In (A) and (D), the color map shows the log fraction of the ocean volume with [Si] and [Zn] that fall within 1 μM by 0.1 nM bins. In (B), (C), (E), and (F), dots are observed [Zn] ± 1 S.D. (*4*, *9*, *13*, *31*) and lines are corresponding model results, averaged within small spatial regions (*15*).

(Fig. 1D). Model sensitivity tests indicate that neither hydrothermal Zn inputs (*17*) nor spatially varying remineralization scales of organic matter (*18*) can resolve the discrepancy (fig. S5). A candidate hypothesis, supported by laboratory culture studies, is that Zn is reversibly "scavenged" (adsorbed) onto sinking organic particles, enhancing its flux to the deep ocean relative to nonscavenged elements like P (*9*).

We investigated whether a second model configuration that explicitly includes reversible scavenging (*15*) can reconcile the Si-like distribution of Zn with its P-like remineralization behavior. The model computes the equilibrium partitioning of uncomplexed Zn between the dissolved phase and a phase adsorbed to sinking particulate organic matter based on a globally uniform partition coefficient (*19*) and does not consider potential adsorption to mineral phases. Following parameter optimization, this model successfully reproduces the observed tight correlation between Zn and Si (R^2 = 0.98) without leaving systematic biases (Fig. 2D). Although Zn concentrations in the surface Southern Ocean remain relatively unchanged from the original model (Fig. 2E), scavenging redistributes Zn from intermediate to deep water masses as they age, bringing its simulated depth structure in line with observations (Fig. 2F and fig. S3). This occurs even though only a small fraction of total Zn is adsorbed onto particles: ~0.5% in the upper ocean and <0.01% in the deep ocean (fig. S6). Overall, resolving reversible scavenging reduces the root mean square error between simulated

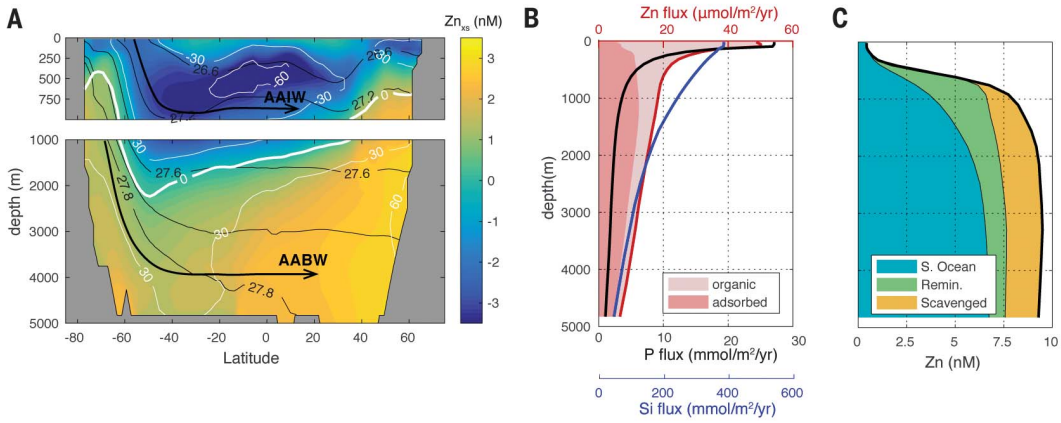

Fig. 3. Holistic understanding of the model Zn cycle. (**A**) The stoichiometric tracers Zn_{xs} (color map) and Si_{xs} (white contours) measure the excess or deficit of Zn and Si relative to PO_4^{3-} and illustrate the relationship between the three nutrient cycles in our model. Both tracers show distinctive signatures circulated by AAIW and AABW from the Southern Ocean and similar modifications along isopycnals outside of the Southern Ocean. (**B**) Vertical flux profiles of P, Si, and Zn. Organic Zn attenuates over depth like P, but adsorbed and organic components sum to a flux profile that is more similar to Si. (**C**) Simulated North Pacific Zn (site analyzed in Fig. 1) is divided into a component circulated from the Southern Ocean and components accumulated from remineralization and scavenging.

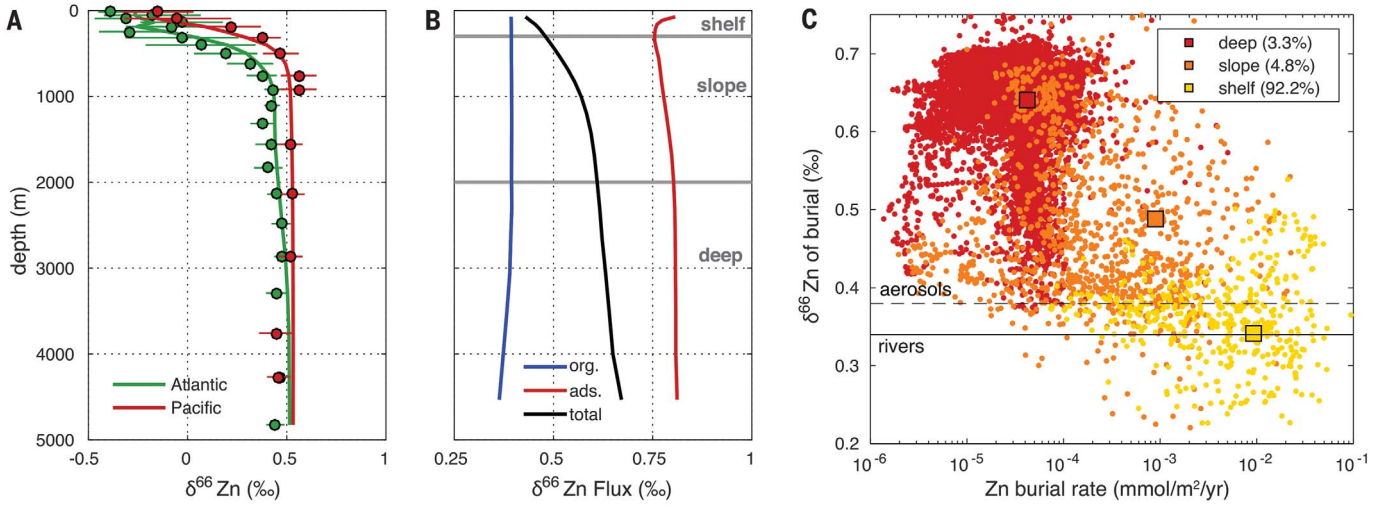

Fig. 4. Zn isotope distribution and mass balance. (**A**) Model fit to observed δ^{66}Zn profiles in the Atlantic and Pacific Oceans. (**B**) Simulated isotopic composition of organic, adsorbed, and total particulate fluxes. The decrease in δ^{66}Zn toward the surface in (A) results from the flux of heavy adsorbed Zn to the deep ocean. (**C**) Relationship between Zn burial rate in sediments, computed offline from high-resolution topography and estimates of carbon burial (*15*), and δ^{66}Zn of the flux to seafloor. Square symbols integrate across shelf (0 to 200 m), slope (200 to 2000 m), and deep ocean (>2000 m) regions. Most burial occurs in shallow shelf regions, where light organic Zn dominates the sinking flux (B), allowing the total δ^{66}Zn sink to match the source from aerosol and river inputs.

and observed Zn by a factor of ~2 relative to the original model (0.59 nM versus 1.03 nM) (table S3). Additionally, inclusion of scavenging permits realistic surface depletion without the excessive Zn:P export ratios seen in our earlier model (Fig. 2E and fig. S4). Model sensitivity tests demonstrate that reversible scavenging must be active throughout the water column, and not confined to low-oxygen waters, to best match the observations (fig. S5). This suggests that the scavenging mechanism is not related to trace metal sulfide precipitation in particle microenvironments (*20*), which might be more important at smaller scales and for other metals, such as cadmium.

By linking Southern Ocean water masses with reversible scavenging, our model provides a holistic understanding of the oceanic Zn cycle and its relationships to Si and PO_4^{3-}. The roles of physical and biogechemical processes can be isolated using stoichiometric tracers that measure the excess or deficit of Zn and Si relative to PO_4^{3-}. Here, we define $Zn_{xs} = [Zn]\text{-}R_{Zn:P}[PO_4^{3-}]$ and $Si_{xs} = [Si]\text{-}R_{Si:P}[PO_4^{3-}]$, where $R_{Zn:P}$ and $R_{Si:P}$ represent mean-ocean elemental ratios. Nutrient utilization in the Southern Ocean surface produces water masses with distinct stoichiometries that are conserved by circulation: AAIW carries strongly negative Zn_{xs} (–1.5 nM) and Si_{xs} (–40 μM) into low latitudes, whereas deeper AABW carries weakly positive values (Fig. 3A).

Modification of these tracers along circulation pathways reflects biogeochemical processes that decouple Zn and Si from PO_4^{3-}. Si_{xs} decreases in AAIW as it ages equatorward and increases in AABW (Fig. 3A), reflecting remineralization of P in intermediate waters and excess Si remineralization in the deep ocean (Fig. 3B) (*11*). Zn_{xs} undergoes almost identical modifications (Fig. 3A) but via a different set of mechanisms. In the upper ~400 m, where organic Zn remineralizes rapidly like P, net adsorption transfers dissolved Zn onto particles (Fig. 3B), constituting a sink of Zn_{xs}. Deeper, the equilibrium between adsorbed and dissolved Zn shifts due to lower particle concentrations, driving net desorption and accumulation of Zn, relative to PO_4^{3-} in AABW (Fig. 3A). Outside the Southern Ocean, the combined flux profiles of organic and adsorbed Zn are more similar to Si than P, with ~30% of Zn transferred from the base of the euphotic zone to 2000 m, compared with ~40% and ~5% for Si

and P, respectively (Fig. 3B). By the time AABW reaches the North Pacific Ocean, the accumulation of desorbed Zn adds ~2 nM to the concentration leaving the Southern Ocean in AABW, compared with ~1 nM accumulated from remineralization (Fig. 3C), demonstrating that reversible scavenging is a critical process explaining the deep accumulation of Zn (Fig. 1D).

In our optimized model, removing the reversible scavenging process and preventing elevated uptake of Zn in the Southern Ocean degrade the fit to observations to a similar degree (*15*). This suggests that both processes are equally responsible for decoupling the Zn distribution from other soft-tissue nutrients and its global similarity to Si. Nevertheless, in young water masses that have not undergone extensive scavenging, shallow remineralization of Zn can locally decouple its concentration from Si (fig. S3), as observed in the subarctic North Pacific Ocean (*21*), although the mechanism for this decoupling was not previously clear.

The existence of distinct organic and adsorbed sinking Zn phases might also resolve an apparent conflict between the vertical distribution of Zn isotopes and the isotopic mass balance of the ocean as a whole. In the low-latitude ocean, the ratio of ^{66}Zn to ^{64}Zn (expressed as δ^{66}Zn) decreases toward the surface, implying preferential removal of heavy isotopes from the upper ocean and their transfer to depth (Fig. 4A) (*22*). However, light isotopes must be preferentially buried from the ocean as a whole to balance fluvial, atmospheric, and hydrothermal sources that are isotopically light [0.3 to 0.35 per mil (‰)] relative to mean-ocean Zn (~0.5‰) (*23*).

We expanded our global model to distinguish the cycles of ^{66}Zn and ^{64}Zn—which are fractionated during biological uptake, complexation, and scavenging (*15*)—and the magnitude of each fractionation effect was optimized within reasonable ranges to match observed δ^{66}Zn profiles (Fig. 4A and fig. S7). In the optimal model, ^{66}Zn is preferentially adsorbed onto sinking particles due to its weaker binding by ligands, consistent with culture studies (*9*) and new observations from the subtropical Pacific (*15*). This fractionation is strongest in the upper 1000 m where ligand binding is most complete (figs. S6 and S8). The flux of heavy adsorbed Zn from the upper ocean then leaves a light δ^{66}Zn signature that is transferred into sinking organic matter when phytoplankton consume residual Zn in the surface (Fig. 4B and fig. S8). The δ^{66}Zn of the sinking Zn flux is therefore light (<0.5‰) in the upper ~500 m, where organic Zn dominates, and heavy (>0.5‰) in deeper layers where the adsorbed flux is dominant (Fig. 4B). Because particulate matter is disproportionately buried on shallow continental shelves (*24*), our model predicts a negative relationship between δ^{66}Zn flux to the seafloor and burial rate (Fig. 4C and fig. S9) (*15*), consistent with observations of light Zn burial on Pacific shelves (*25*). Integrated globally, this yields a δ^{66}Zn sink of 0.36 ± 0.04‰, which is in balance with source estimates (*23*).

Our findings have important implications for Zn biogeochemical cycling in past and future oceans. The geological record exhibits millennial cycles (*26*, *27*) and billion-year trends (*28*) in δ^{66}Zn, currently attributed to Zn speciation and changes in biological productivity. Our findings suggest that changes in the relative burial of adsorbed and organic Zn are an important mechanism controlling mean-ocean δ^{66}Zn on geological time scales. In the modern ocean, deep remineralization of Si and reversible scavenging of Zn produce similar accumulation patterns of the two nutrients, but these processes likely have different sensitivities to ocean change. Whereas Si cycling will respond to changing ocean temperature and pH (*29*), Zn will be sensitive to projected variations in organic carbon fluxes (*30*) that underpin Zn scavenging, potentially decoupling the Zn and Si supply to low-latitude phytoplankton communities.

REFERENCES AND NOTES

1. B. S. Twining, S. B. Baines, *Ann. Rev. Mar. Sci.* **5**, 191–215 (2013).
2. F. M. M. Morel *et al.*, *Nature* **369**, 740–742 (1994).
3. K. W. Bruland, G. A. Knauer, J. H. Martin, *Nature* **271**, 741–743 (1978).
4. E. Mawji *et al.*, *Mar. Chem.* **177**, 1–8 (2015).
5. C. Mahaffey, S. Reynolds, C. E. Davis, M. C. Lohan, *Front. Mar. Sci.* **1**, 73 (2014).
6. Y. Shaked, Y. Xu, K. Leblanc, F. M. M. Morel, *Limnol. Oceanogr.* **51**, 299–309 (2006).
7. W. G. Sunda, S. A. Huntsman, *Limnol. Oceanogr.* **37**, 25–40 (1992).
8. M. J. Ellwood, K. Hunter, *Limnol. Oceanogr.* **45**, 1517–1524 (2000).
9. S. G. John, T. M. Conway, *Earth Planet. Sci. Lett.* **394**, 159–167 (2014).
10. B. Twining *et al.*, *Limnol. Oceanogr.* **59**, 689–704 (2014).
11. M. Holzer, F. W. Primeau, T. DeVries, R. Matear, *J. Geophys. Res. Oceans* **119**, 313–331 (2014).
12. D. Vance *et al.*, *Nat. Geosci.* **10**, 202–206 (2017).
13. Y. Zhao, D. Vance, W. Abouchami, H. J. W. de Baar, *Geochim. Cosmochim. Acta* **125**, 653–672 (2014).
14. J. L. Sarmiento, N. Gruber, M. A. Brzezinski, J. P. Dunne, *Nature* **427**, 56–60 (2004).
15. Materials and methods are available as supplementary materials.
16. T. Kim, H. Obata, Y. Kondo, H. Ogawa, T. Gamo, *Mar. Chem.* **173**, 330–341 (2015).
17. S. Roshan, J. Wu, W. Jenkins, *Mar. Chem.* **183**, 25–32 (2016).
18. T. Weber, J. A. Cram, S. W. Leung, T. DeVries, C. Deutsch, *Proc. Natl. Acad. Sci. U.S.A.* **113**, 8606–8611 (2016).
19. M. P. Bacon, R. F. Anderson, *J. Geophys. Res.* **87**, 2045–2056 (1982).
20. D. J. Janssen *et al.*, *Proc. Natl. Acad. Sci. U.S.A.* **111**, 6888–6893 (2014).
21. D. J. Janssen, J. T. Cullen, *Mar. Chem.* **177**, 124–133 (2015).
22. T. M. Conway, S. G. John, *Global Biogeochem. Cycles* **28**, 1111–1128 (2014).
23. S. H. Little, D. Vance, C. Walker-Brown, W. M. Landing, *Geochim. Cosmochim. Acta* **125**, 673–693 (2014).
24. J. P. Dunne, J. L. Sarmiento, A. Gnanadesikan, *Global Biogeochem. Cycles* **21**, GB4006 (2007).
25. S. H. Little, D. Vance, J. McManus, S. Severmann, *Geology* **44**, 207–210 (2016).
26. S. Pichat, C. Douchet, F. Albarede, *Earth Planet. Sci. Lett.* **210**, 167–178 (2003).
27. M. Kunzmann *et al.*, *Geology* **41**, 27–30 (2013).
28. M. L. Pons *et al.*, *Geobiology* **11**, 201–214 (2013).
29. M. A. Brzezinski, D. M. Nelson, *Deep Sea Res. Part I Oceanogr. Res. Pap.* **42**, 1215–1237 (1995).
30. L. Bopp *et al.*, *Biogeosciences* **10**, 6225–6245 (2013).
31. S. G. John, J. Helgoe, E. Townsend, *Mar. Chem.* **2017**, 10.1016/j.marchem.2017.06.003 (2017).

ACKNOWLEDGMENTS

We thank R. Bundy and D. Repeta for providing organic Zn samples from the North Pacific for isotope analysis. **Funding:** This work was supported by NSF (OCE-1658042 to T.W., OCE-1649439 and OCE-1658436 to S.J., and OCE-1658392 to T.D.), NERC (NE/N001079/1 to A.T.), and the Simons Foundation (329108 to S.J.). **Author contributions:** T.W. and S.J. designed the study and developed the biogeochemical model. T.D. developed the ocean circulation model. T.W., S.J., and A.T. interpreted the model output. All authors contributed to writing the paper. **Competing interests:** None declared. **Data and materials availability:** Data used in this paper are presented in the supplementary materials or available from the GEOTRACES archive (www.geotraces.org/). The ocean circulation model is available from www.geog.ucsb.edu/~devries/Home/Models.html.

SUPPLEMENTARY MATERIALS

www.sciencemag.org/content/361/6397/72/suppl/DC1
Materials and Methods
Supplementary Text
Figs. S1 to S9
Tables S1 to S3
References (*32*–*52*)

1 September 2017; accepted 11 May 2018
10.1126/science.aap8532

Biological uptake and reversible scavenging of zinc in the global ocean

Thomas Weber, Seth John, Alessandro Tagliabue and Tim DeVries

Science **361** (6397), 72-76.
DOI: 10.1126/science.aap8532

Controlling zinc in the oceans

Zinc, a key micronutrient for marine phytoplankton, has a global distribution remarkably similar to that of silicic acid, even though Zn and Si have very different biogeochemical cycles. Weber *et al.* investigated why this is so by combining model calculations and observations. They found that biological uptake in the Southern Ocean and reversible scavenging of Zn onto sinking particles both affect the distribution of Zn in the ocean. Thus, Zn and Si distributions will be affected differently by future changes in ocean temperature, pH, and carbon fluxes.

Science, this issue p. 72